Gradual Transformation of Ag₂S to Au₂S Nanoparticles by Sequential Cation Exchange Reactions: Binary, Ternary and Hybrid Compositions

Mariona Dalmases,[†,#] Pau Torruella,[⊥,#] Javier Blanco-Portals,[⊥,#] Albert Vidal,[†,#] Miguel Lopez-Haro,[‡]

José Juan Calvino,[‡] Sònia Estradé,[⊥,#] Francesca Peiró[⊥,#] and Albert Figuerola*[,†,#]

[†] Departament de Química Inorgànica i Orgànica, Secció de Química Inorgànica, Universitat de Barcelona, Martí i Franquès 1-11, 08028 Barcelona, Spain

[#] Institut de Nanociència i Nanotecnologia (IN2UB), Universitat de Barcelona, Martí i Franquès 1-11, 08028 Barcelona, Spain

[⊥] Laboratory of Electron Nanoscopies (LENS)-MIND/IN2UB, Departament d'Electrònica, Universitat de Barcelona, Martí i Franquès 1-11, 08028 Barcelona, Spain

[‡] Departamento de Ciencia de los Materiales e Ingeniería Metalúrgica y Química Inorgánica, Facultad Ciencias, Universidad de Cádiz, Campus Rio San Pedro, Puerto Real, 11510 Cádiz, Spain

ABSTRACT: Cation exchange reactions have been exploited in the last years as an efficient tool for the controlled chemical modification of pre-made nanocrystals. In this work, the gradual transformation of Ag₂S nanocrystals into Au₂S analogues is performed by sequential cation exchange reactions that allow for a fine control of the chemical composition, delivering also two intermediate ternary sulfides based exclusively on noble metals. The role of two different surfactants in the reaction medium has been studied: while dodecylamine is favoring the heterogeneous nucleation of metallic Au on the surface of the semiconductor domains in detriment of the cation exchange reaction, the use of tetraoctylammonium bromide turns out to be crucial for the enhancement of the exchange in order to reach full cation substitution, if desired. The presence of Br⁻ anions in the reaction medium represents an additional tool to modulate the morphology of the final nanocrystals, being either solid or hollow depending on their concentration. The synthetic protocol has been successfully conducted in both spherical and rod-like nanocrystals with identical results, leading to a wide variety of binary, ternary and/or hybrid nanostructures that have been carefully characterized.

INTRODUCTION

Chemical approaches offer many strategies for the control of matter at the nanoscale. Among them, solution-based processes have revealed as highly valuable techniques to tailor not only size, but morphology and chemical composition of nanostructures as well. Nanocrystals with anisotropic shapes and engineered compositions have been successfully prepared in the last years by exploiting surfactant-assisted preferential growth reactions, galvanic replacement processes and cation exchange phenomena among others[1–4] Cation exchange reactions stand out by far as one of the most representative examples of this paradigm, through which many nanostructured materials have been chemically modified under soft conditions in solution while fully preserving their size and shape, circumventing in this way the need to develop direct and elaborate synthetic protocols of materials for which this might represent a struggling task.[5] In particular, the direct synthesis of ternary or quaternary materials entails the search of multiple precursor and reactive species that are prompt to react and decompose at the same temperature and with similar kinetics in order to assure the homogeneous formation of the final nanoparticles (NPs).[6] Alternatively, performing partial cation exchange in a controlled manner in simple parental binary materials can lead to the formation of multielement materials with a high degree of homogeneity even at low temperatures when appropriate precursors are used.[7–9]

Chalcogenide-based semiconductor nanostructures have strongly benefited from cation displacement processes: Alivisatos and coworkers pioneered this field already in 2004 by reporting for the first time the possibility to exploit cation exchange reactions as a chemical transformation tool at the nanoscale for a few chalcogenide materials.[10] Later in 2007 the same group envisaged further limits of this post-synthetic approach and confirmed the possibility to perform non-homogeneous cation exchange reactions on CdS nanorods, leading to segmented and elongated superlattices formed by alternating CdS and Ag₂S domains.[11] From that moment many groups have devoted their efforts to expand these strategies to other materials and also to investigate the critical factors underlying the mechanisms of such reactions.[12–15]

The importance of structural and morphological parameters, the influence of the oxidation state and coordination environment of the outgoing and incoming ions, and the presence of appropriate precipitating and/or complexing agents that might significantly alter the thermodynamics of an otherwise unfavorable exchange reaction are among the subjects explored in the

Scheme 1. Experimental reaction conditions used for the direct preparation of the nanostructures presented (solid lines) and reaction mechanism followed for their formation (dashed lines).
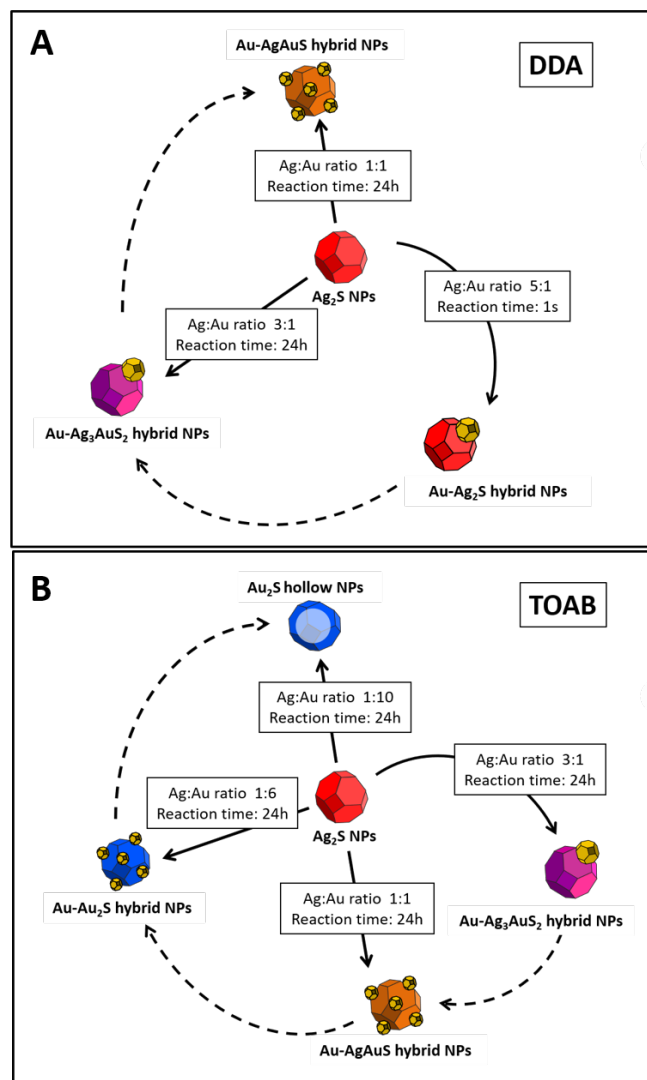
most recent years.[16–20] Considering and controlling all these factors become specially critical when cation exchange competes with other potential reactions. In particular when intending to exchange a cation species by another cation of a metal with high electron affinity like Au, in which full reduction to metallic Au can easily occur, avoiding the cation substitution desired, if reaction conditions are not accurately controlled.[21]

Noble metal chalcogenides are a new class of materials that have been only recently studied. In particular, binary silver chalcogenides have been reported as near infrared (NIR) absorbers and emitters as well as potential thermoelectric energy converters. Our group made a step forward regarding these environmentally-friendly materials by exploring the Ag_2Se phase diagram at the nanoscale when introducing gold as a third element in the structures, in an attempt to enlarge the availability of new materials without compromising the low toxicity of the parental binary material.[22] Our previous results showed how cation exchange reactions, in combination with metal heterogeneous nucleation, opened the door for the synthesis of a set of diverse nanocrystals that turned out to show potential as thermoelectric energy conversion materials, as

well as contrast agents for Computed Tomography diagnostic techniques, when appropriately functionalized.[22,23] In this work we describe the synthesis of the analogous ternary system with sulphur. Compared to the Ag/Au/Se system where only one single ternary material exists that is called *fischisserite* and shows a Ag_3AuSe_2 stoichiometry, the S analogue presents two possible stoichiometric compounds, namely the Ag_3AuS_2 (*uytenbogaardtite*) and the AgAuS (*petrovskaite*), both previously studied as bulk from compositional, structural, thermodynamic and electronic perspectives by other authors.[24–30] Such structural and stoichiometry diversity represents a new challenge for cation exchange procedures in colloidal systems. Our results show that cation exchange reactions can be successfully performed on Ag_2S nanocrystals in order to obtain pure Ag_3AuS_2 and AgAuS nanocrystals decorated with metallic Au. Additionally, further exchange is possible and metastable Au_2S nanocrystals, both solid and hollow, can also be prepared by carefully controlling the occurrence of the Kirkendall effect.[31] A reaction mechanism is proposed for the formation of such collection of new nanoitems.

EXPERIMENTAL SECTION

Chemicals. Sulfur powder (S, 99.99%) was obtained from Strem Chemicals. Silver nitrate ($AgNO_3$, 99%), gold (III) chloride trihydrate ($HAuCl_4 \cdot 3H_2O$, ≥99.9%), oleylamine (OLAm, 70%), dodecylamine (DDA, 98%), tetraoctylammonium bromide (TOAB, 98%) and toluene (99.9%) were purchased from Sigma-Aldrich. Ethanol (EtOH, 96% v/v) was obtained from Panreac. All the reagents and solvents were used without further purification.

Synthesis of Ag_2S NPs. The synthesis of Ag_2S NPs was adapted from that published by Wang and co-workers.[32] 17 mg $AgNO_3$ (0.1 mmol), 8 mg S (0.25 mmol) and 8 mL OLAm were placed in a three-neck flask and were purge three times by vacuum-N_2 cycles. Under N_2 atmosphere, the system was heated to 160°C and let it react for 20 minutes at this temperature. The colour of the solution was changing slowly from orange to dark brown. After this time, the heating was removed, and the solution was let cool down naturally. Once the solution was at room temperature, NPs were precipitated by the addition of EtOH and centrifugation (4 minutes at 4500 rpm), finally the precipitate was dispersed in toluene. In order to fully preserve the colloidal stability of NPs and completely avoid their partial aggregation, the sample should be washed only once.

Synthesis of Ag_2S nanorods. For the synthesis of Ag_2S nanorods the procedure described for Jang and co-workers was used.[33] Under inert atmosphere, sulphur precursor solution was prepared dissolving 50 mg S (1.56 mmol) in 7 mL OLAm, slightly heating was necessary for the complete dissolution of the solid. This solution was injected to a three-neck flask under nitrogen and temperature was raised to 100°C. Once this temperature was reached, silver precursor was injected and the mixture reacted for 2 minutes at this temperature. After this time, the heating mantle was removed and the solution was let cool down naturally. The mixture was extracted to a vial with 2 mL of toluene and, 2 mL of ethanol were added to destabilize the dispersion and precipitate the NPs. After 3 minutes of centrifugation at 4500 rpm, supernatant was discarded and the precipitate was re-dispersed in toluene.

Silver precursor solution was prepared dissolving 50 mg Ag-NO$_3$ (0.29 mmol) in 2 mL OLAm at temperature above 200°C. Heating the solution was important, because having metallic silver instead of Ag(I) was essential for obtaining elongated nanostructures.

Phase transfer of Au(III) cations from water to toluene. The phase transfer of Au(III) cations from water to toluene was done following the protocol reported by Yang and co-workers.[34] In order to obtain a 6 mM Au(III)-DDA stock solution, 60 mg (0.15 mmol) HAuCl$_4$·3H$_2$O dissolved in 25 mL of deionized water were mixed with an ethanolic solution of dodecylamine (2.4 g (13 mmol) DDA in 25 mL EtOH). The aqueous solution, which was transparent and orange, became translucent after the mixture with the ethanolic solution. After 3 minutes of stirring, 25 mL of toluene were added to the solution, and the stirring was kept for 3 more minutes. After the separation of the two phases, the toluene phase was extracted and washed three times with 10 mL of H$_2$O/EtOH 1:1 mixture to avoid the precipitation of silver chloride in further reactions with silver sulphide NPs. The Au-DDA stock solution should be prepared and used immediately after, since after approximately 3 days of storage, the formation of small Au nanoparticles was observed in the solution. The preparation of 6 mM Au(III)-TOAB stock solution was also adapted from this protocol, using 187.5 mg (0.34 mmol) of TOAB instead of DDA. The Au-TOAB stock solution was stable at least during 4 or 5 months without any Au reduction occurring, indicating the weaker reduction character of the quaternary TOAB ammonium salt with respect to the aliphatic primary DDA amine.

Synthesis of Ag-Au-S hybrid nanostructures

For the synthesis of complex nanostructures made of Ag, Au and S a simple reaction at room temperature was used in all cases. The procedure consisted in the mixture of 300 µL of pre-synthesised Ag$_2$S NPs (0.6µM) with the Au(III)-TOAB/DDA solution. The conditions used in the different syntheses are shown in Table 1 and Scheme 1. When the concentration of NPs and Au precursor in the reaction medium is well controlled, the synthetic strategy is highly reproducible.

Table 1: Reaction conditions for the synthesis of Ag-Au-S hybrid nanostructures

Product	Surfac-tant*	V$_{Au}$ solution*	Ag:Au ratio	t$_{reaction}$
Au-Ag$_3$AuS$_2$ hybrid NPs	TOAB/DDA	0.6 mL	~3:1	24h
Au-AgAuS hybrid NPs	TOAB/DDA	1.2 mL	~1:1	24h
Au-Ag$_2$S hybrid NPs	DDA	0.3 mL	~5:1	1s
Au-Au$_2$S hybrid NPs	TOAB	8.1 mL	~1:5	24h
Au$_2$S hollow NPs	TOAB	16.2 mL	~1:10	24h

*The concentration of the Au stock solution is 6mM in Au atoms, independently of the surfactant used for the synthesis; the concentration of the TOAB and DDA surfactants in the Au stock solution is 13.6 mM and 520 mM, respectively.

Characterization methods

Transmission electron microscopy (TEM). Samples were prepared for observation by dilution in toluene followed by sonication. A droplet of the solution was then poured in holey carbon covered copper TEM grids. A JEOL 2000 FX II conventional TEM operating an accelerating voltage of 80kV was used.

X-Ray diffraction (XRD). The spectra were acquired with a PANanalytical X'Pert Pro MPD Alpha1 diffractometer operating in θ/2θ geometry at 45 kV, 40 mA, and λ= 1.5406 Å (Cu Kα1). Thin layers of the samples were prepared by drop casting and evaporation of the solvent on a monocrystalline Si holder of 15 mm diameter and 0.15 mm height. Scans in the range 2θ = 4−100° were run at a step size of 2θ = 0.017°and 100 s per step. The data were treated with X'Pert HighScore Plus software.

High Resolution TEM (HRTEM), Electron Diffraction and High Angular Annular Dark Field (HAADF) imaging were performed in a Jeol 2010F operating at 200kV equipped with a FEG gun and a GIF spectrometer.

Electron Tomography. The high-angle annular dark field (HAADF) images for the tomographic reconstruction were acquired in a ThermoFisher TITAN aberration corrected microscope at 80keV, belonging to the Universidad de Cádiz. The angles of the tilt series ranged between +70º and -70º, with an angular step of 5º. The reconstruction was carried out through compressed sensing algorithms, specifically, total variation minimization in 3 dimensions (TVM3D).[35]

Vis-NIR Absorption Spectroscopy. Vis-NIR absorption spectra of all samples were recorded in toluene solution on a Perkin Elmer LAMBDA 950 spectrophotometer.
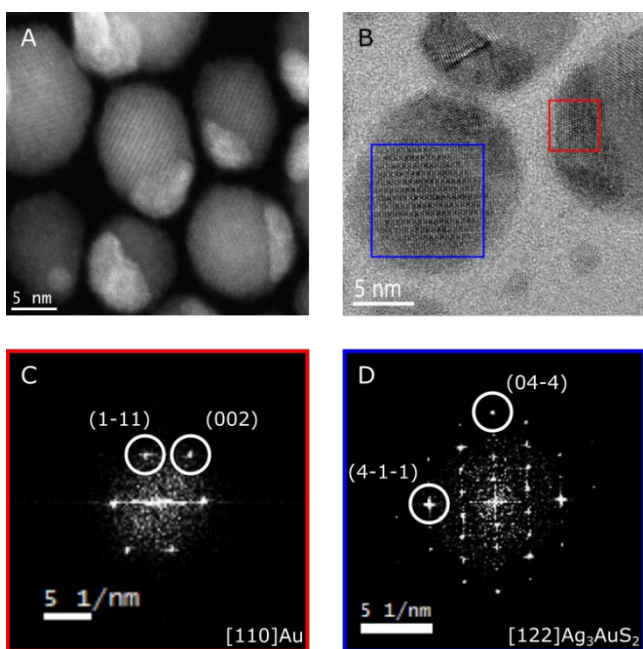
RESULTS AND DISCUSSION

Ag$_2$S precursor NPs

Ag$_2$S NPs were prepared by following a heat-up method reported by Wang and co-workers.[32] Briefly AgNO$_3$ and elemental sulphur were dissolved in OLAm. Ag$_2$S NPs nucleated at 160°C under inert atmosphere and they were allowed to grow during 20 min after which the heating mantle was removed. The high reproducibility, the ease of the procedure as well as its efficient scale-up are among its main advantages. Faceted NPs with an average cross-section of 12 nm were obtained, as shown in the TEM micrograph in Figure 1A. Although most of the NPs show a homogeneous contrast under the electron beam, a small population evidences the presence of a tiny domain at the surface of the particle showing a darker contrast. Ag$_2$S can show three crystallographic phases depending on temperature: α-Ag$_2$S, *acanthite*, with a monoclinic crystal structure stable at low temperatures below 177°C; β-Ag$_2$S, *argentite*, a super-ionic conductor with cubic symmetry usually observed in the range between 177 and 586°C, and γ-Ag$_2$S, a high-temperature cubic phase, stable at temperatures above 586°C.[36] As reflected in the XRD spectrum in Figure 1G, the nanocrystals showed the expected *acanthite* monoclinic structure, and no peaks corresponding to secondary phases could be observed. HRTEM analysis confirmed the previous structure as the main phase in the sample (Figure 2 A-B) but it also revealed the presence of a few NPs in lower frequency whose interplanar distances matched with a high temperature cubic phase of Ag$_2$S (Figure 2 C-D). The stabilization of unexpected phases at the nanoscale has often been reported as a result of the energy balance derived from
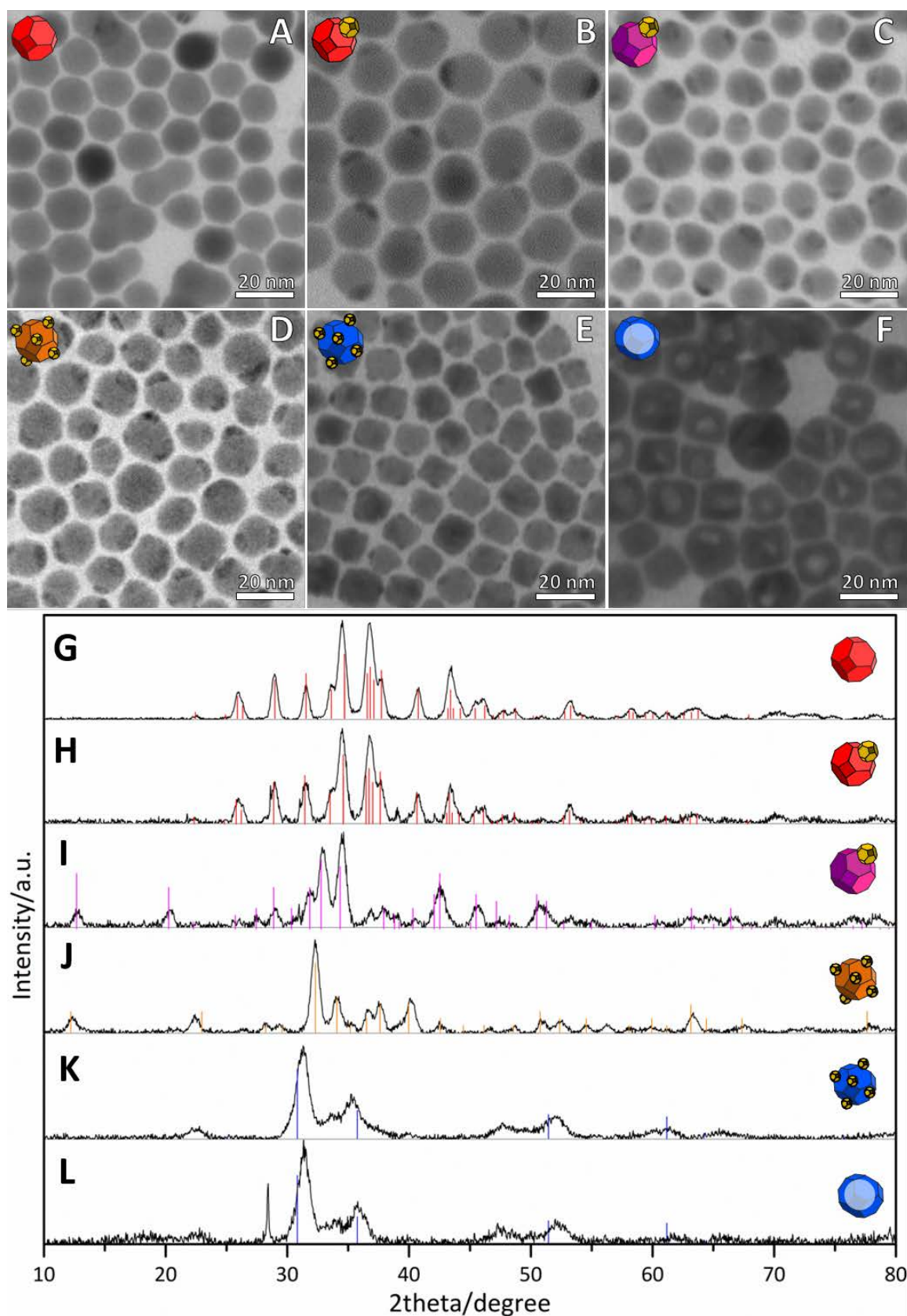
Figure 1: TEM micrographs of (A) Ag$_2$S NPs, (B) Au-Ag$_2$S hybrid NPs, (C) Au-Ag$_3$AuS$_2$ hybrid NPs, (D) Au-AgAuS hybrid NPs, (E) Au-Au$_2$S hybrid NPs and, (F) Au$_2$S hollow NPs. XRD patterns of (G) Ag$_2$S NPs, (H) Au-Ag$_2$S hybrid NPs, (I) Au-Ag$_3$AuS$_2$ hybrid NPs, (J) Au-AgAuS hybrid NPs, (K) Au-Au$_2$S hybrid NPs and, (K) Au$_2$S hollow NPs. XRD reference patterns: monoclinic Ag$_2$S (JCPDS 024-0715, red), tetragonal Ag$_3$AuS$_2$ (JCPDS 020-0461, pink), monoclinic AgAuS (JCPDS 038-0396, orange) and, cubic Au$_2$S (JCPDS 085-1997, blue).
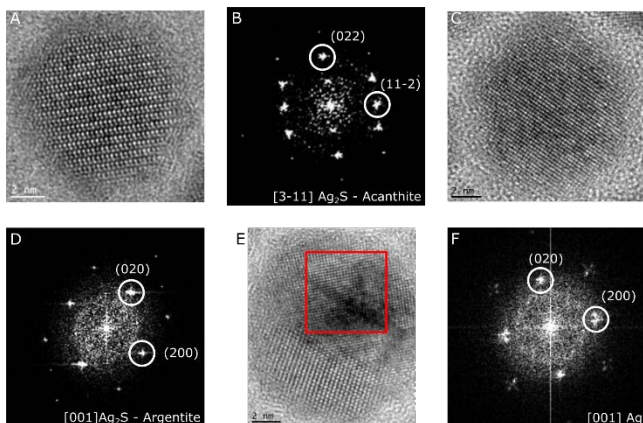
Figure 2. Ag$_2$S precursor NPs characterization. (A) HRTEM image from the average *acanthite* NP. (B) FFT from panel A). (C) HRTEM image from a rare *argentite* NP. (D) FFT from panel C). (E) HRTEM image of a rare hybrid Ag-Ag$_2$S NP. (F) FFT from the red region of panel E).
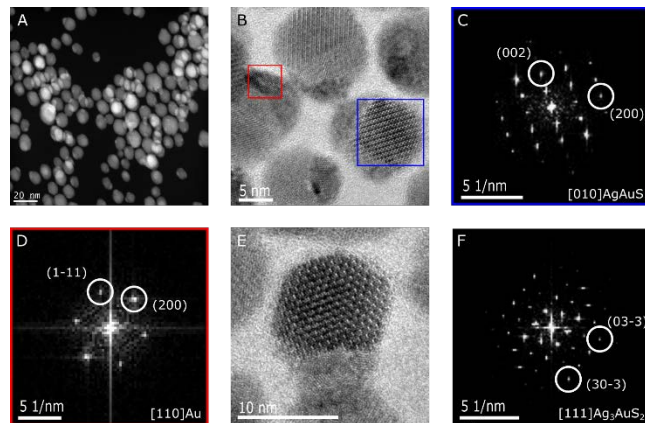

Figure 4. Au-AgAuS Hybrid NPs characterization. (A) HAADF image. (B) HRTEM image of the Au-AgAuS hybrid NPs. (C) FFT from the blue region of panel B), indexed as *petrovskaite*. (D) FFT from the red region of panel B), indexed as gold. (E) HRTEM image of a rare Au-Ag$_3$AuS$_2$ hybrid NP. (F) FFT from panel E).

Figure 3. Au-Ag$_3$AuS$_2$ Hybrid NPs characterization. (A) HAADF image. (B) HRTEM image of the Au-Ag$_3$AuS$_2$ hybrid NPs. (C) FFT from the red region of panel B), indexed as gold. (D) FFT from the blue region of panel B), indexed as *uytenbogaardtite*.

high surface-to-volume ratio particles.[37] Additionally, HRTEM allowed to identify the presence of small metallic Ag domains on the surface of a few NPs (Figure 2E-F), corresponding to the dark spots observed already at low magnification TEM images.
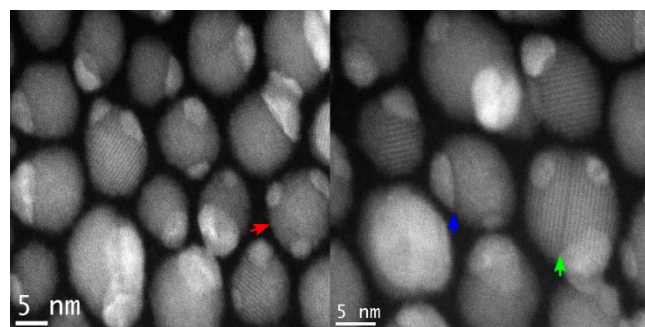
The Ag$_2$S nanorods synthesis was adapted from the method published by Son and co-workers in 2007.[33] TEM micrographs shown in Figure S1 in the SI evidence the high monodispersity of the sample that consists of rods of 50 nm length and 10 nm width in average. XRD spectra confirmed the monoclinic crystalline phase as in the previous hexagonal NPs. In addition, HRTEM and FFT analyses (Figure S2 in the SI) fully agreed with the previous characterization.

### Ag$_2$S-based Ternary Semiconductor NPs

Our strategy consists on mixing a particular amount of colloidally stable Ag$_2$S NPs with a specific amount of Au(III)-

Figure 5. HAADF images of Au-AgAuS hybrid NPs. The red arrow highlights a NP with multiple gold domains; the blue one, the amorphous interface appearing as a dark fringe surrounding the gold domains; the green one a defect on an AgAuS crystal.
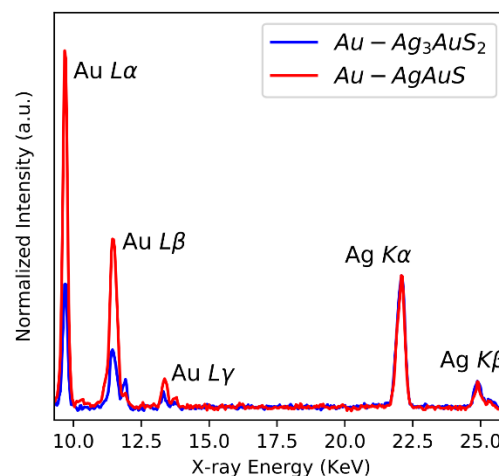
Figure 6. EDX spectra from the Au-Ag$_3$AuS$_2$ and Au-AuAuS samples. Background has been subtracted and spectra have been normalized by the intensity of the Ag Kα peak.

surfactant complexes, both in toluene, and leaving the mixture under constant mechanical stirring during 24 h at room temperature. Two different surfactants were used in our experiments, namely TOAB and DDA, although no significant

differences were found in the products obtained with both of them at this stage.

Our experiments indicated that the atomic Ag:Au ratio in the mixture was the most critical parameter in order to control the stoichiometry of the ternary material obtained. Figures 1C and 1D show TEM micrographs of the samples prepared with a Ag:Au ratio of 3:1 and 1:1. As observed, NPs have preserved their average dimensions and shape in both cases. However, the growth of a secondary domain with a darker contrast was obvious at the surface of all NPs synthesized with a Ag:Au ratio of 3:1, which evolved to the formation of several analogous but smaller domains when the ratio was increased to 1:1. XRD was used in order to confirm the phases and purity of the samples. As shown in Figures 1I and 1J, a reaction mixture with a Ag:Au ratio of 3:1 led unambiguously to a pure tetragonal lattice corresponding to the Ag_3AuS_2 ternary material, while a 1:1 ratio quantitatively transformed the structure to a monoclinic lattice that belongs to the AgAuS ternary material. No traces of the precursor monoclinic Ag_2S lattice were found in the XRD patterns of the two samples, as well as no mixture of the two ternary systems was detected. Same results were obtained when Ag_2S rod-like NPs were used (Figure S3 and S4).

HRTEM and HAADF images reflect the same results that have been shown in TEM images described in previous paragraph. Specifically, the product obtained with a Ag:Au ratio of 3:1 consists of dimer-like NPs (Figure 3). STEM-HAADF images (Figure 3A) demonstrate the two distinct domains of the NPs. The smaller domain is brighter, meaning it is made of heavier elements, consistent with it being metallic gold, whereas the domain of darker contrast, lighter, may be *uytenbogaardtite* (Ag_3AuS_2). These surmises were proved by HRTEM analyses (Figure 3B-D), where the results of both domains clearly matched with the supposed materials. Apart from that, a barrier of darker contrast is observed between the two domains of the dimers. This and the clear lack of epitaxy seen in the HRTEM images, evidence an amorphous interface between the domains.

HRTEM images of the product obtained with a Ag:Au ratio of 1:1 (Figure 4) were also consistent with previous TEM and XRD results. Most NPs had more than one gold domain and the semiconductor domain was mainly AgAuS, as evidenced in the STEM-HAADF (Figure 4A) and HRTEM measurements (Figure 4B-D). Nevertheless, it was found with further HRTEM analyses that there were remains of Ag_3AuS_2 (Figures E-F), which gave an idea of the mechanism of the reaction as will be discussed later. HAADF images of the sample are shown in Figure 5. As it was mentioned before, these images are useful to identify nanostructures with multiple domains. Red arrow in right image shows a NP with more than one domain of gold. HRTEM analyses showed no epitaxy between the Au and the semiconductor domain in the NPs, and thus Au is not growing on specific crystallographic sites of the semiconductor section. In agreement with that, the energy required for the heterogeneous nucleation of Au is likely quite similar independently of the crystallographic facet where it occurs. Thus, when the concentration of Au precursor is increased, Au can easily nucleate in different facets/sites leading to several Au domains per NP, while when the concentration of Au precursor is low like in the case of Au-Ag_3AuS_2 sample, the growth of only the first nucleus is favored compared to further nucleation events. In the HAADF images in Figure 5, the boundary between the gold and the semiconductor domains can also be seen (blue arrow in left image), as well as some defects in the semiconductor crystals (green arrow in left image shows a planar defect). Although these defects were also seen in the previous sample, they were more frequent in the current one.

EDX analyses of these two samples were carried out. Different punctual spectra and averaged scans from wider areas were acquired for each sample. The spectra were quantified, and the average results showed the mean composition of Ag-Au-S crystals of each sample. Whereas sample derived from a Ag:Au ratio of 3:1 had 75±2% of silver and 25±2% of gold, sample derived from a Ag:Au ratio of 1:1 had 54±2% of silver and 46±2% of gold. These results agreed perfectly with the stoichiometry of the two ternary materials. Figure 6 shows the aver-aged spectra for both samples.

Suppressing and Enhancing Cation Exchange

So far, the methodology reported led to the preparation of hybrid and ternary Au-Ag_3AuS_2 and Au-AgAuS nanocrystals, confirming the ability of cation exchange reactions to control quantitatively the final stoichiometry of the product obtained. Nevertheless, new reaction conditions were tested in order to either suppress or enhance the exchange further, in an attempt to establish the limits of this approach within the Ag/Au/S system. The choice of TOAB or DDA as a surfactant revealed as crucial for this purpose. On the one hand, long chain alkylamines are well known for their reducing character in the synthesis of metallic NPs.[38] Thus, it could be envisaged that the use of DDA could allow for the preparation of Au-Ag_2S hybrid NPs where the parental semiconductor domain has not suffered any chemical transformation. Indeed, the reaction of Ag_2S NPs in toluene with Au(III)-DDA complexes in a Ag:Au ratio of 3:1 was enough as to obtain dimeric NPs as the ones shown in Figure 1B, where the semiconductor domain had fully preserved the starting monoclinic binary Ag_2S structure as indicated by the XRD spectrum in Figure 1H. However, the reaction time must be limited to a few seconds by immediately precipitating the sample after the mixture of the reactive species, in order to completely suppress the cation exchange and the formation of ternary structures.

On the other hand, cation exchange requires only partial reduction of Au(III) to Au(I) and its subsequent solid state diffusion through the NPs. Such process strongly competes with the full reduction to metallic Au, which should be minimized. Based on this, the use of ternary alkylamines as surfactants is clearly detrimental and TOAB was used as an alternative. Experiments were performed by increasing the Ag:Au ratio to 1:5 and 1:10 and by keeping constant the rest of reaction conditions. In the first case, cubic-shaped NPs were obtained which were decorated with multiple small domains of darker contrast as observed in Figure 1E. The change of shape of the starting hexagonal NPs to the nearly cubic final nanocrystals clearly indicated that the semiconductor domain had suffered a significant transformation. XRD measurements indicated that this transformation was not only morphological but also chemical, and con-firmed that the Ag_2S NPs underwent full cation exchange leading to a metastable Au_2S phase with a cubic structure (see Figure 1K). Additionally, when a Ag:Au ratio of 1:10 was used in the experiment, cubic-shaped Au_2S NPs with a hollow morphology were obtained like those shown in Figure 1F, which structure was determined by XRD
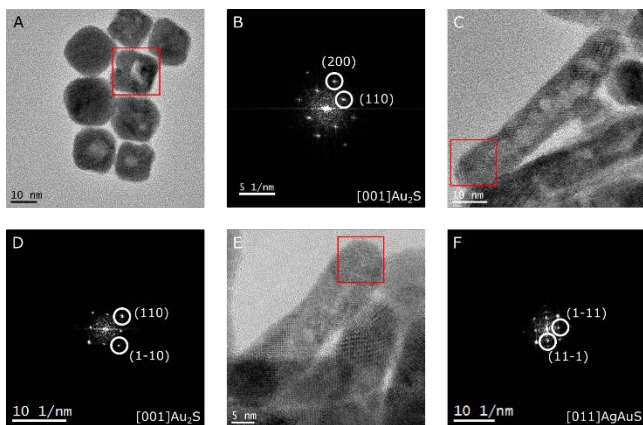
Figure 7. (A) HRTEM image of spherical hollow Au_2S NPs. (B) Indexed FFT from the highlighted region in A). (C) HRTEM image of rod-shaped hollow Au_2S NPs. (D) Indexed FFT from the highlighted region in C). (E) HRTEM image of spherical rod-shaped Au_2S NPs. (F) Indexed FFT from the highlighted region in E).

measurements and are shown in Figure 1L. Identical results were observed when using rod-like Ag_2S NPs as starting sample. Representative TEM micrographs of hollow Au_2S nanorods are shown in Figure S5 of the SI. Both hollow spherical (Figure 7A-B) and rod-like (Figure 7C-D) samples were studied by HRTEM: FFT analysis. The results agreed well with the conclusions extracted from XRD, although some minor portions of the monoclinic AgAuS ternary phase could also be identified (Figure 7E-F). Additionally, the measurements showed that Au_2S cubes are faceted by (100) planes.

The tomographic reconstructions of the hollow Au_2S nanorods were conducted in two different areas at two different magnifications. The coexistence of void and solid rods is observed in the two different cases. The reconstruction showed that while some of the voids are totally included inside the rods, as seen by consecutive slices in Figure 8F, others are partial exclusions, as seen in the consecutive slices of Figure 8C. Thus, what initially seemed as a simple mixture of solid rods and core-shell like structures, results in a complex geometry problem where several different morphologies coexist.

Reaction mechanism

The results described in this work evidence the presence of a strong competition between two different chemical pathways. One of them entails the full reduction of Au(III) cations to metallic Au and further heterogeneous nucleation of the noble metal at the surface of the semiconductor NP. The other involves a partial reduction of Au(III) to Au(I) ions followed by solid state diffusion and cation exchange reaction within the semiconductor domain. The competition can be unbalanced to one side or another by the presence of specific chemical species. As in our previous work with the analogous Ag_2Se system, the presence of alkylamines like DDA perceptibly enhances the first pathway favoring the formation of dimeric hybrid NPs where the formation of ternary materials can be entirely suppressed under certain conditions. On the contrary, and due to the lack of non-bonding electron pairs, the use of a quaternary alkylamine bromide like TOAB seems to partially hamper this process in benefit of the cation exchange reaction. Similarly in previous reports, CdS nanorods were partially transformed into Au_2S_x/CdS nanorods by cation exchange reactions in water in complete absence of reducing

agents,[21] while the heterogeneous growth of metallic Au on the surface of cadmium or silver chalcogenide quantum dots has been traditionally assisted by long chain alkylamines as the only reducing agents.[39,40]

The presence of bromide anions in the medium significantly alters the kinetics of the process by promoting the exchange reaction pathway: halide precipitating agents act as an external driving force for the removal of native Ag(I) cations, as confirmed by the precipitation of AgBr in all samples where cation exchange took place, detected by XRD (see Figure S6 of the SI). White and microcrystalline AgBr powder can be easily removed from the solution by gently centrifuging the reaction mixture and decanting the supernatant containing the desired colloidal sample. Then the dark brown solution can be further washed from excess organics by usual precipitation-redissolution cycles. Although AgBr can be quantitatively removed from the nanocrystalline sample, it has been occasionally encountered and identified by HRTEM analysis as seen in Figure S7.

The heterogeneous nucleation of Au seems completely
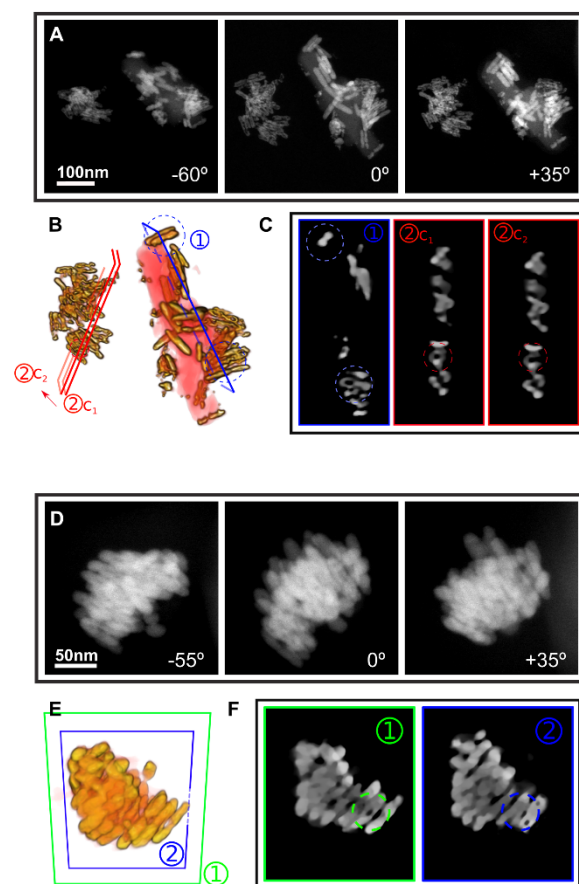
Figure 8. (A) Three HAADF projections of the first area acquired: -60, 0 and +35 degrees. (B) Volume rendering of the first area reconstructed. (C) Slices of the volume reconstructed in areas of interest (where several inclusions and exclusions on the rods were present. The slices correspond to the areas marked in (B) with the same colors and labels. (D) Three HAADF projections of the second area acquired at higher magnification: -55, 0 and +35 degrees. (E) Volume rendering of the second area reconstructed. (F) Slices of the volume reconstructed in areas of interest.

inevitable in the S-based system even when using TOAB as surfactant, contrary to the Se-based system case where ternary Ag_3AuSe_2 NPs without metallic Au domains could be easily isolated under similar reaction conditions.[22] This fact suggests the presence of a stronger reducing environment in the current system and this will be discussed later. The extent of cation exchange achievable constitutes another important dissimilarity between the two analogous systems: the Ag/Au/S ternary phase diagram indicates a much higher miscibility of the three elements giving rise to a wider variety of structures and stoichiometries including not only the tetragonal Ag_3AuS_2 compound, but also the monoclinic AgAuS alloy. Surprisingly, the formation of Ag/Au/S alloyed nanostructures is lacking in most of the reports working with this ternary system,[40,41] even when metallic Au diffusion is tracked through a Ag_2S domain from a core to a surface position.[42] As the only two exceptions, Liu et al. and Li et al. recently reported on ternary NPs obtained from the progressive sulphurization of AgAu alloy colloids, although an in-depth characterization was not performed in these cases.[43,44] Furthermore, cation exchange reactions can be performed to completion in this system, obtaining Au_2S nanostructures whose formation is most likely stabilized thanks to the covalency of the Au-S bond that shows a binding energy 2 eV higher than that of the Ag-S in the parental Ag_2S, as reported by Morris et al.[45] Again, the presence of bromide anions in the medium plays a key role in defining the final morphology of the fully exchanged Au_2S NPs by accelerating the outwards diffusion of Ag(I) cations in the reaction medium with the highest concentration of Br(-I) anions, which leads to the formation of hollow nanostructures due to the slower Au(I) inwards diffusion, following the Kirkendall mechanism.[31] Probably the hollow morphology could not be achieved in the case of the Se-based system since maximum one out of four Ag(I) ions could be exchanged and therefore very few vacancies are generated so as to create a hole in the Ag_3AuSe_2 NPs. Au_2S has been described as a p-type semiconductor with a direct bandgap estimated between the visible and near-infrared region of the electromagnetic spectrum.[46,47] In combination with other materials, it has been suggested as an interesting light harvesting, catalytic, biosensing or therapeutic component.[48–51] It crystallizes in the cubic crystal system with a cuprite-type structure, being isostructural at room temperature to the high conductivity ionic conductor α-Ag_2S.[46] It is reported to be a highly metastable phase, decomposing both under inert atmosphere and air conditions at temperatures above 420 K, and its preparation often leads to amorphous solids, with a few exceptions at the nanoscale.[46,52–54] It is worth mentioning that the crystallinity of the Au_2S nanostructures reported here is highly preserved at room temperature for months after preparation. Additionally, spherical and rod-like Au_2S NPs with a hollow morphology like the ones described in this work have not been reported to date and, after appropriate functionalization and water transfer, they open up the doors for the use of such *a priori* biocompatible elongated nanostructures as potential nanocontainers for dual diagnostic and therapeutic applications, in line with our recent studies about biomedical applications of noble metal-based chalcogenides analogous to the ones described in this work.[23]

The results described here confirm a gradual and finely controlled cation exchange on Ag_2S NPs. A Ag:Au ratio of 3:1 is required to obtain pure Ag_3AuS_2 domains, while 1:1 and 1:5 ratios are necessary for AgAuS and Au_2S phases, respectively. Ratios in between lead inevitably to a mixture of phases and

compositions, which confirm that the NPs undergo a gradual structural and chemical transition until the final compound is obtained. The gradual cation exchange is also accompanied by an increasing number of structural defects, as it can be concluded from both XRD and HRTEM analysis (Figures 1 and 5): XRD shows increasing width of peaks with the growing amount of Au(I) in the structure, while in HRTEM micrographs several defects can be observed as the cation exchange proceeds.

The question still remains on which is the main Au(III) reducing agent in these systems: the reaction mixtures contain oleylamine-capped Ag_2S NPs, and Au(III)-TOAB or Au(III)-DDA reactive species dissolved in toluene. At first glance, DDA is expected to be the most reducing species, although experiments point out that Au(III) is reduced to Au(I) and even to Au(0) also in TOAB and complete absence of DDA. We therefore suggest two possible Au(III) reducing agents, based on the reactive species present in the medium and our previous observations: on the one hand, oleylamine molecules working as stabilizing agents already coordinated at the surface of pre-synthesized Ag_2S NPs; on the other hand the S(-II) anion of the inorganic crystal lattice. In the Se analogue we observed that the Se(-II) was working as a sacrificial anion to reduce Au(III) to Au(I), and indeed an amorphous Se layer was observed surrounding ternary NPs.[22] In fact, HRTEM micrographs also point to the formation of a thin amorphous shell after the cation exchange reaction (Figures 3 and 5). Although in principle, S(-II) should be less reducing than Se(-II), experimentally the nucleation of Au(0) is observed in all samples prepared with S and could not be avoided, contrary to what happens with Se. All in all, and regardless of its origin, the reduction of Au(III) could be significantly enhanced due to the possibility of formation of both thermodynamically favored Au(I)-S(-II) and Au(0)-S(-II) bonds, as reported by other authors.[45]

The optical absorption was measured in solution in the Visible and NIR range for all the samples prepared and it is shown in Figure 9. The initial Ag_2S NPs and the final hollow Au_2S NPs show an exponential and continuous absorption profile at wavelengths below 750 nm, where no absorption bands are visible. As expected, Au-Ag_3AuS_2 and Au-AgAuS hybrid NPs show a broad and intense absorption band centered between
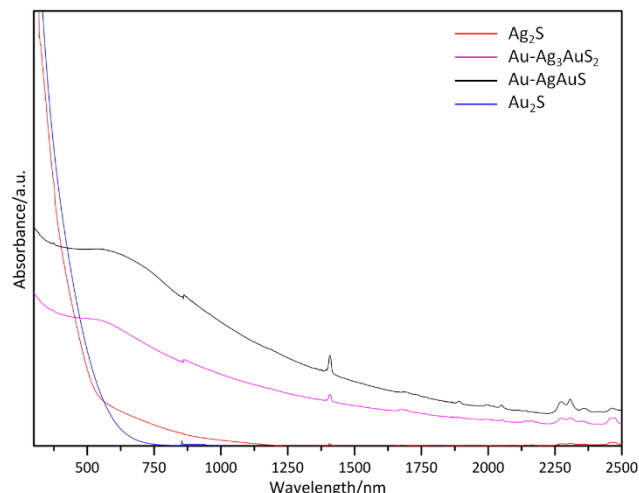
Figure 9. Vis-NIR absorbance spectra of Ag_2S NPs, Au-Ag_3AuS_2 HNPs, Au-AgAuS HNPs and Au_2S hollow NPs.

500 and 600 nm corresponding to the metallic Au Surface Plasmon Resonance band.

CONCLUSIONS

Our studies evidence the high miscibility of Au in the binary Ag-S system due to the strong affinity of Au and S elements and the thermodynamic stability of their bond. A wide range of nanostructured materials is presented with controlled and known compositions, going from Ag_2S to Au_2S at the extremes, as well as two additional ternary intermediate compositions, i.e. Ag_3AuS_2 and $AgAuS$. The transformation occurs through finely tuned cation exchange reactions that provoke gradual changes in composition without significantly altering the size and shape of the precursor Ag_2S NPs. The role of two different surfactants in the reaction medium has been studied: while dodecylamine is favoring the heterogeneous nucleation of metallic Au on the surface of the semiconductor domains in detriment of the cation exchange reaction, the use of TOAB turns out to be crucial for the enhancement of the exchange in order to reach even full cation substitution. Bromide anions reveal themselves as an efficient external driving force for the removal of Ag(I) cations from the solid lattice, which prefer to precipitate as microcrystalline AgBr. On the other hand, bromide anions play a key role in determining the solid or hollow morphology of the nanostructures obtained by controlling the outgoing diffusion speed of Ag(I) cations. In this way, hollow Au_2S NPs both with a spherical or rod-like shape have been prepared and fully characterized, as they represent promising nanocontainers for dual diagnostic and therapeutic applications.

ASSOCIATED CONTENT

Supporting Information. TEM micrograph and XRD pattern of Ag_2S nanorods; HRTEM image and FFT of Ag_2S nanorods; TEM micrographs and XRD of Au-Ag_3AuS_2 and Au-$AgAuS$ hybrid nanorods; HRTEM images of Au_2S hollow nanorods; Identification of AgBr by XRD and HRTEM. This material is available free of charge via the Internet at http://pubs.acs.org.

AUTHOR INFORMATION

Corresponding Author

*E-mail: albert.figuerola@ub.edu

Notes
The authors declare no competing financial interests.

ACKNOWLEDGMENT

REFERENCES

(1) Carbone, L.; Nobile, C.; De Giorgi, M.; Della Sala, F.; Morello, G.; Pompa, P.; Hytch, M.; Snoeck, E.; Fiore, A.; Franchini, I. R.; *et al.* Synthesis and Micrometer-Scale Assembly of Colloidal CdSe/CdS Nanorods Prepared by a Seeded Growth Approach. *Nano Lett.* **2007**, *7*, 2942–2950.

(2) Moreau, L. M.; Schurman, C. A.; Kewalramani, S.; Shahjamali, M. M.; Mirkin, C. A.; Bedzyk, M. J. How Ag Nanospheres Are Transformed into AgAu Nanocages. *J. Am. Chem. Soc.* **2017**, *139*, 12291–12298.

(3) Song, G.; Liang, C.; Gong, H.; Li, M.; Zheng, X.; Cheng, L.; Yang, K.; Jiang, X.; Liu, Z. Core-Shell MnSe@Bi2Se3 Fabricated via a Cation Exchange Method as Novel Nanotheranostics for Multimodal Imaging and Synergistic Thermoradiotherapy. *Adv. Mater.* **2015**, *27*, 6110–6117.

(4) Anderson, B. D.; Tracy, J. B. Nanoparticle Conversion Chemistry: Kirkendall Effect, Galvanic Exchange, and Anion Exchange. *Nanoscale* **2014**, *6*, 12195–12216.

(5) Gupta, S.; Kershaw, S. V.; Rogach, A. L. 25th Anniversary Article: Ion Exchange in Colloidal Nanocrystals. *Adv. Mater.* **2013**, *25*, 6923–6944.

(6) Aldakov, D.; Lefrançois, A.; Reiss, P. Ternary and Quaternary Metal Chalcogenide Nanocrystals: Synthesis, Properties and Applications. *J. Mater. Chem. C* **2013**, *1*, 3756–3776.

(7) Akkerman, Q. A.; Genovese, A.; George, C.; Prato, M.; Moreels, I.; Casu, A.; Marras, S.; Curcio, A.; Scarpellini, A.; Pellegrino, T.; *et al.* From Binary Cu2S to Ternary Cu-In-S and Quaternary Cu-In-Zn-S Nanocrystals with Tunable Composition via Partial Cation Exchange. *ACS Nano* **2015**, *9*, 521–531.

(8) Tan, J. M. R.; Scott, M. C.; Hao, W.; Baikie, T.; Nelson, C. T.; Pedireddy, S.; Tao, R.; Ling, X.; Magdassi, S.; White, T.; *et al.* Revealing Cation-Exchange-Induced Phase Transformations in Multielemental Chalcogenide Nanoparticles. *Chem. Mater.* **2017**, *29*, 9192–9199.

(9) Van der Stam, W.; Geuchies, J. J.; Altantzis, T.; Van Den Bos, K. H. W.; Meeldijk, J. D.; Van Aert, S.; Bals, S.; Vanmaekelbergh, D.; De Mello Donega, C. Highly Emissive Divalent-Ion-Doped Colloidal CsPb1-XMxBr3 Perovskite Nanocrystals through Cation Exchange. *J. Am. Chem. Soc.* **2017**, *139*, 4087–4097.

(10) Son, D. H.; Hughes, S. M.; Yin, Y.; Alivisatos, P. A. Cation Exchange Reactions in Ionic Nanocrystals. *Science (80-.).* **2004**, *306*, 1009–1012.

(11) Robinson, R. D.; Sadtler, B.; Demchenko, D. O.; Erdonmez, C. K.; Wang, L.-W.; Alivisatos, A. P. Spontaneous Superlattice Formation in Nanorods through Partial Cation Exchange. *Science* **2007**, *317*, 355–358.

(12) Luther, J. M.; Zheng, H.; Sadtler, B.; Alivisatos, A. P. Synthesis of PbS Nanorods and Other Ionic Nanocrystals of Complex Morphology by Sequential Cation Exchange Reactions. *J. Am. Chem. Soc.* **2009**, *131*, 16851–16857.

(13) Li, H.; Zanella, M.; Genovese, A.; Povia, M.; Falqui, A.; Giannini, C.; Manna, L. Sequential Cation Exchange in Nanocrystals: Preservation of Crystal Phase and Formation of Metastable Phases. *Nano Lett.* **2011**, *11*, 4964–4970.

(14) Bothe, C.; Kornowski, A.; Tornatzky, H.; Schmidtke, C.; Lange, H.; Maultzsch, J.; Weller, H. Solid-State Chemistry on the Nanoscale: Ion Transport through Interstitial Sites or Vacancies? *Angew. Chemie - Int. Ed.* **2015**, *54*, 14183–14186.

(15) White, S. L.; Smith, J. G.; Behl, M.; Jain, P. K. Co-Operativity in a Nanocrystalline Solid-State Transition. *Nat. Commun.* **2013**, *4*, 1–8.

(16) Casavola, M.; Van Huis, M. A.; Bals, S.; Lambert, K.; Hens, Z.; Vanmaekelbergh, D. Anisotropic Cation Exchange in PbSe/CdSe Core/Shell Nanocrystals of Different Geometry. *Chem. Mater.* **2012**, *24*, 294–302.

(17) Miszta, K.; Gariano, G.; Brescia, R.; Marras, S.; De Donato, F.; Ghosh, S.; De Trizio, L.; Manna, L. Selective Cation Exchange in the Core Region of Cu2-XSe/Cu2-XS Core/Shell Nanocrystals. *J. Am. Chem. Soc.* **2015**, *137*, 12195–12198.

(18) Tu, R.; Xie, Y.; Bertoni, G.; Lak, A.; Gaspari, R.; Rapallo, A.; Cavalli, A.; Trizio, L. De; Manna, L. Influence of the Ion Coordination Number on Cation Exchange Reactions with Copper Telluride Nanocrystals. *J. Am. Chem. Soc.* **2016**, *138*, 7082–7090.

(19) De Trizio, L.; Li, H.; Casu, A.; Genovese, A.; Sathya, A.; Messina, G. C.; Manna, L. Sn Cation Valency Dependence in Cation Exchange Reactions Involving Cu2-XSe Nanocrystals. *J. Am. Chem. Soc.* **2014**, *136*, 16277–16284.

(20) De Trizio, L.; Manna, L. Forging Colloidal Nanostructures via Cation Exchange Reactions. *Chem. Rev.* **2016**, *116*, 10852–10887.

(21) Kundu, S.; Kundu, P.; Van Tendeloo, G.; Ravishankar, N. Au2Sx/CdS Nanorods by Cation Exchange: Mechanistic Insights into the Competition between Cation-Exchange and

Metal Ion Reduction. *Small* **2014**, *10*, 3895–3900.

(22) Dalmases, M.; Ibáñez, M.; Torruella, P.; Fernàndez-Altable, V.; López-Conesa, L.; Cadavid, D.; Piveteau, L.; Nachtegaal, M.; Llorca, J.; Ruiz-Gonzàlez, M. L.; *et al.* Synthesis and Thermoelectric Properties of Noble Metal Ternary Chalcogenide Systems of Ag-Au-Se in the Forms of Alloyed Nanoparticles and Colloidal Nanoheterostructures. *Chem. Mater.* **2016**, *28*, 7017–7028.

(23) Caro, C.; Dalmases, M.; Figuerola, A.; García-Martín, M. L.; Leal, M. P. Highly Water-Stable Rare Ternary Ag-Au-Se Nanocomposites as Long Blood Circulation Time X-Ray Computed Tomography Contrast Agents. *Nanoscale* **2017**, *9*, 7242–7251.

(24) Barton, M. D. The Ag-Au-S System. *Econ. Geol.* **1980**, *75*, 303–316.

(25) Seryotkin, Y. V; Bakakin, V. V; Pal, G. A.; Kokh, K. A. Synthesis and Crystal Structure of the Trigonal Silver (I) Dithioaurate(I), Ag3AuS2. *Cryst. Growth Des.* **2011**, *11*, 1062–1066.

(26) Bindi, L.; Stanley, C.; Seryotkin, Y.; Bakakin, V.; Pal'yanova, G.; Kokh, K. The Crystal Structure of Uytenbogaardtite, Ag 3 AuS 2 , and Its Relationships with Gold and Silver Sulfides-Selenides. *Mineral. Mag.* **2016**, *80*, 1031–1040.

(27) Seryotkin, Y. V.; Bakakin, V. V.; Pal'yanova, G. A.; Kokh, K. A. Synthesis and Crystal Structure of Silver–gold Sulfide AgAuS. Four-Fold Interpenetrated Three-Dimensional [(Au,Ag)10S8]-Networks. *CrystEngComm* **2014**, *16*, 1675–1680.

(28) Osadchii, E. G.; Rappo, O. A. Determination of Standard Thermodynamic Properties of Sulfides in the Ag-Au-S System by Means of a Solid-State Galvanic Cell. *Am. Mineral.* **2004**, *89*, 1405–1410.

(29) Gurevich, V. M.; Gavrichev, K. S.; Osadchii, E. G.; Tyurin, A. V.; Ryumin, M. A. Heat Capacity and Thermodynamic Functions of Petrovskaite (AgAuS) at 0–583 K and Mineral Equilibria in the Ag-Au-S System. *Geochemistry Int.* **2011**, *49*, 422–428.

(30) Mikhlin, Y. L.; Nasluzov, V. A.; Romanchenko, A. S.; Shor, A. M.; Pal'Yanova, G. A. XPS and DFT Studies of the Electronic Structures of AgAuS and Ag3AuS2. *J. Alloys Compd.* **2014**, *617*, 314–321.

(31) Wang, W.; Dahl, M.; Yin, Y. Hollow Nanocrystals through the Nanoscale Kirkendall Effect. *Chem. Mater.* **2013**, *25*, 1179–1189.

(32) Wang, J.; Feng, H.; Chen, K.; Fan, W.; Yang, Q. Solution-Phase Catalytic Synthesis, Characterization and Growth Kinetics of Ag2S-CdS Matchstick-like Heteronanostructures. *Dalt. Trans.* **2014**, *43*, 3990–3998.

(33) Jang, K.; Kim, S. Y.; Park, K. H.; Jang, E.; Jun, S.; Son, S. U. Shape-Controlled Synthesis of Silver Sulfide Nanocrystals by Understanding the Origin of Mixed-Shape Evolution. *Chem. Commun.* **2007**, 4474–4476.

(34) Yang, J.; Sargent, E. H.; Kelley, S. O.; Ying, J. Y. A General Phase-Transfer Protocol for Metal Ions and Its Application in Nanocrystal Synthesis. *Nat. Mater.* **2009**, *8*, 683–689.

(35) López-Haro, M.; Tinoco, M.; Fernández-Garcia, S.; Chen, X.; Hungria, A. B.; Cauqui, M. Á.; Calvino, J. J. A Macroscopically Relevant 3D-Metrology Approach for Nanocatalysis Research. *Part. Part. Syst. Charact.* **2018**, *35*, 1–11.

(36) Sharma, R. C.; Chang, Y. A. The Ag-S (Silver-Sulfur) System. *Bull. Alloy Phase Diagrams* **1986**, *7*, 263–269.

(37) Soriano, R. B.; Arachchige, I. U.; Malliakas, C. D.; Wu, J.; Kanatzidis, M. G. Nanoscale Stabilization of New Phases in the PbTe-Sb2Te 3 System: PbmSb2 NTem +3 n Nanocrystals. *J. Am. Chem. Soc.* **2013**, *135*, 768–774.

(38) Newman, J. D. S.; Blanchard, G. J. Formation of Gold Nanoparticles Using Amine Reducing Agents. *Langmuir* **2006**, *22*, 5882–5887.

(39) Mokari, T.; Rothenberg, E.; Popov, I.; Costi, R.; Banin, U. Selective Growth of Metal Tips onto Semiconductor Quantum Rods and Tetrapods. *Science* **2004**, *304*, 1787–1790.

(40) Yang, J.; Ying, J. Y. Room-Temperature Synthesis of Nanocrystalline Ag2S and Its Nanocomposites with Gold. *Chem. Commun.* **2009**, *1*, 3187–3189.

(41) Yang, J.; Ying, J. Y. Nanocomposites of Ag2S and Noble Metals. *Angew. Chemie - Int. Ed.* **2011**, *50*, 4637–4643.

(42) Yang, J.; Ying, J. Y. Diffusion of Gold from the Inner Core to the Surface of Ag2S Nanocrystals. *J. Am. Chem. Soc.* **2010**, *132*, 2114–2115.

(43) Liu, M.; Zeng, H. C. General Synthetic Approach to Heterostructured Nanocrystals Based on Noble Metals and I-VI, II-VI, and I-III-VI Metal Chalcogenides. *Langmuir* **2014**, *30*, 9838–9849.

(44) Li, X.; Schaak, R. E. Reactive AgAuS and Ag3AuS2 Synthons Enable the Sequential Transformation of Spherical Nanocrystals into Asymmetric Multicomponent Hybrid Nanoparticles. *Chem. Mater.* **2017**, *29*, 4153–4160.

(45) Morris, T.; Copeland, H.; Szulczewski, G. Synthesis and Characterization of Gold Sulfide Nanoparticles. *Langmuir* **2002**, *18*, 535–539.

(46) Ishikawa, K.; Isonaga, T.; S, W.; Suzuki, Y. Structure and Electrical Properties of Au2S. *Solid State Ionics* **1995**, *79*, 60–66.

(47) Suárez, J. A.; Plata, J. J.; Márquez, A. M.; Sanz, J. F. Structural, Electronic and Optical Properties of Copper, Silver and Gold Sulfide: A DFT Study. *Theor. Chem. Acc.* **2016**, *135*, 1–8.

(48) Wolf, A.; Kodanek, T.; Dorfs, D. Tuning the LSPR in Copper Chalcogenide Nanoparticles by Cation Intercalation, Cation Exchange and Metal Growth. *Nanoscale* **2015**, *7*, 19519–19527.

(49) Gadgil, B.; Damlin, P.; Viinikanoja, A.; Heinonen, M.; Kvarnström, C. One-Pot Synthesis of an Au/Au 2 S Viologen Hybrid Nanocomposite for Efficient Catalytic Applications. *J. Mater. Chem. A* **2015**, *3*, 9731–9737.

(50) Liu, Y.; Ma, Y.; Zhou, J.; Li, X.; Xie, S.; Tan, R. Sythesis, Modification, and Biosensing Characteristics of Au2S/AuAgS-Coated Gold Nanorods. *J. Nanomater.* **2015**, *2015*, 1–8.

(51) Gobin, A. M.; Watkins, E. M.; Quevedo, E.; Colvin, V. L.; West, J. L. Near-Infrared-Resonant Gold/Gold Sulfide Nanoparticles as a Photothermal Cancer Therapeutic Agent. *Small* **2010**, *6*, 745–752.

(52) Kuo, C.; Huang, M. H. Hydrothermal Synthesis of Free-Floating Au 2 S Nanoparticle Superstructures. *J Phys Chem C* **2008**, *112*, 11661–11666.

(53) Wang, X.; Liu, X.; Zhu, D.; Swihart, M. T. Controllable Conversion of Plasmonic Cu 2−x S Nanoparticles to Au 2 S by Cation Exchange and Electron Beam Induced Transformation of Cu 2−x S–Au 2 S Core/Shell Nanostructures. *Nanoscale* **2014**, *6*, 8852–8857.

(54) Hu, C.; Chen, W.; Xie, Y.; Verma, S. K.; Destro, P.; Zhan, G.; Chen, X.; Zhao, X.; Schuck, P. J.; Kriegel, I.; *et al.* Generating Plasmonic Heterostructures by Cation Exchange and Redox Reactions of Covellite CuS Nanocrystals with Au 3+ Ions. *Nanoscale* **2018**, *10*, 2781–2789.